

Received 5 October 2023, accepted 19 October 2023, date of publication 30 October 2023, date of current version 3 November 2023.

Digital Object Identifier 10.1109/ACCESS.2023.3328620

RESEARCH ARTICLE

Active Disturbance Rejection Decoupling Control for Independent-Metering Electro-Hydraulic System With Online Compensation Information

WANG MENG^{id}, LI HUSHAN^{id}, GAO YOUSHAN^{id}, AND XI HAO

School of Mechanical Engineering, Taiyuan University of Science and Technology, Taiyuan 030024, China

Corresponding author: Gao Youshan (gaoyoushan@tyust.edu.cn)

This work was supported in part by the Shanxi Scholarship Council of China under Grant 2020-124, in part by the Natural Science Foundation of Shanxi Province of China under Grant 20210302123217, in part by the Taiyuan University of Science and Technology Innovative Projects in Graduate Education under Grant BY2022012, in part by the Introduction of Talent Research Start-Up Fund of Shanxi Province under Grant 20202062, in part by the Shanxi Province Science Foundation for Youths under Grant 202203021212322, and in part by the Shanxi Center of Technology Innovation for Electrohydraulic Control and Health Management of Heavy Machinery.

ABSTRACT Aiming at the problems of complex operating conditions, large load disturbance, strong coupling of pressure and position control subsystems, and time-varying parameters of independent metering electro-hydraulic servo system (IMEHSS), an active disturbance rejection decoupling (ADRC) control method with online compensation information is proposed in this paper. In this study, the internal coupling of subsystems is treated as the part of total disturbances, and decoupling control is realized by estimating and compensating the total disturbance through extended state observer. In position control subsystem, the cylinder dynamic changes caused by the inlet chamber flow rate of cylinder and the deviation of the nominal calculated flow rate from actual calculated flow rate are calculated in real time. And these calculated values are compensated to the controller as online information to improve the control accuracy and the disturbance rejection ability of position control. By calculating the cylinder velocity in real time to obtain the effect of cylinder speed on the change of return chamber pressure and compensating it into the controller to improve the return chamber pressure control accuracy. The online information compensation method presented in this paper reduces the amount of total disturbance and thus reduces the burden of extended state observer. At the same time, this method can realize the proportional relationship between the regulation parameters and control signals in the passive pressure control subsystem, which simplifies the tuning process of parameters. Finally, to verify the effectiveness and rationality of the method, simulations and experiments are carried out.

INDEX TERMS Active disturbance rejection control, information compensation, independent metering electro-hydraulic servo system, decoupling control, extended state observer.

I. INTRODUCTION

Due to the advantages of, large output force, heavy load tolerance, easy realization of linear and rotational motion, high control accuracy, flexible arrangement of components, high power-weight ratio, and suitable for working in harsh

The associate editor coordinating the review of this manuscript and approving it for publication was Zheng H. Zhu^{id}.

environments, hydraulic systems are extensively used in many fields, such as aerospace, construction machinery [1], [2]. With the huge demand for resources, fossil fuels are being depleted and the energy crisis is intensifying, so it is important to develop hydraulic systems with energy-saving characteristics [3]. As the pressure of return chamber of normal valve-controlled hydraulic cylinder system cannot be regulated, the pressure loss and heat generation of the system

tends to be higher. More and more researchers are focusing on the independent metering technology and applying it to industrial and mobile machinery hydraulic systems to reduce the system energy consumption [4], [5].

Although IMEHSS reduces the system energy consumption and has more flexible control methods, it also increases the complexity of the control system. Guangrong Chen proposed an IARDSC control method, which obtained good trajectory tracking performance and achieved an energy-saving effect through a fast parameter estimation method [6]. Janne Koivumäki designed a modular controller for the independent metering system based on subsystem-dynamics, to ensure system tracking accuracy and reduce actuator energy consumption [7]. In order to solve problems of uncertainties and nonlinearities in IMEHSS, Chen Li proposed an adaptive robust control method which can improve the level of the control precision [8]. Wei Liu proposed a nonlinear coordinated control method for the IMEHSS under sustained negative load to achieve position tracking and smooth speed control of cylinder [9]. Ziqi Liu designed an independent-metering system for hydraulic hexapod robot, and developed a sliding mode repetitive controller for it to get better control performance and energy-saving effect [10]. Aiming at independent metering hydraulic steering system, Qihui Liu designed a combined control strategy based on the position, velocity and pressure of the system to ensure the steering accuracy and achieve the purpose of energy saving [11]. Although some scholars have already studied IMEHS and achieved some results, many advanced control algorithms based on mathematical models are difficult to be widely used in industry which is due to the fact that the hydraulic system is nonlinear and time-varying, and the system is difficult to be represented by an accurate mathematical model [12].

Active disturbance rejection control (ADRC) is a method with the ability of self-resistant which was proposed by Han based on great numbers of engineering practices and theoretical studies. It doesn't depend strictly on the system mathematical model [13]. Although ADRC has not been proposed for a long time, it has been noticed by many scholars and engineers because of its strong active disturbance rejection capability and robustness. Amjad J. Humaidi has applied the ADRC technique to control the position of single-link flexible joint robot manipulator, by comparing the effects of linear and nonlinear ADRC on system characteristics drew the conclusion that the nonlinear ADRC got a better dynamic behavior and the robustness of linear ADRC was better [14]. There are also some scholars who have applied ADRC in various fields [15], [16], [17].

Although ADRC technology is applied in many fields, ADRC is less frequently applied to hydraulic systems. The main reason for this is that the method of ADRC based on the standard extended state observer (ESO) is suitable for the integral chain system that with matching uncertainty [18]. Whereas hydraulic systems have characteristics of mechanical-hydraulic coupling and mismatched uncertainty

inputs. In order to apply ADRC technology in hydraulic servo systems, Chengwen Wang applied singular value perturbation theory to reduce the order of normal valve controlled hydraulic system. At the same time, the model of hydraulic system can be transformed into an integral chain system so that ADRC can be applied directly [19]. Although Chengwen Wang modified the system model, he did not explain how the extended state observer could more accurately observe various states and disturbances in the hydraulic system. And although some academics have begun to study the ADRC control of hydraulic system, they all focused on normal valve-controlled cylinder systems and have not yet carried out research on the application of ADRC to IMEHSS.

As the position and pressure subsystems of IMEHSS have the characteristics of mechanical-hydraulic coupling, in order to realize the separate control of position and return chamber pressure of IMEHSS, to reduce the coupling effect between the two subsystems, and at the same time, to make the system have a good resistance to load interference, an online information compensation ADRC decoupling control method is proposed in this paper. The main contributions of this study can be highlighted as follows:

- (1) Develop mathematical model of IMEHSS including displacement control subsystem and pressure control subsystem.

- (2) Design position ADRC controller with the online compensation information of cylinder dynamic changes that caused by the inlet chamber flow rate of cylinder and the deviation of the nominal calculated flow rate from the actual calculated flow rate.

- (3) Design pressure ADRC controller containing the online compensation information for the effect of cylinder velocity on return chamber pressure.

- (4) By compensating the online information to the controller, the amount of total disturbance is reduced. Thus, this reduces the burden of the observer to estimate the total disturbance, and improve the system control accuracy. And the effectiveness of the proposed method is verified by simulations and experiments.

The rest of this paper is arranged as follows: the mathematical model of IMEHSS is established in section II, section III designs online information compensation ADRC decoupling controller, Co-simulations and experiments are carried out to verify the effectiveness of the method in section IV, finally, conclusions are drawn in section V.

II. ESTABLISHMENT OF MATHEMATICAL MODEL OF IMEHSS

The IMEHSS achieves the purpose of mechanical decoupling of directional valve spool by using different valves to control the flow rate and pressure of cylinder two chambers. Fig. 1 shows the schematic structure of IMEHSS studied in this paper.

The IMEHSS consists mainly of an asymmetric cylinder and two servo directional valves. The areas of rodless

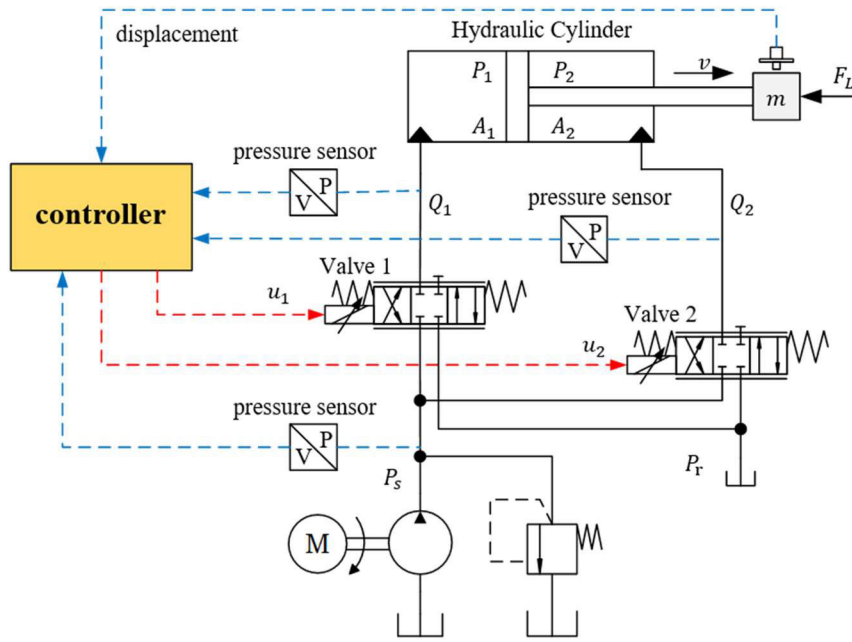


FIGURE 1. Schematic structure of IMEHSS.

chamber and the rod chamber of cylinder are A_1 and A_2 respectively. The pressures of two chambers are P_1 and P_2 , and the oil flow rates of two chambers are Q_1 and Q_2 correspondingly. The controller acquires signals of displacement and pressures, and outputs servo valve control signals u_1 and u_2 at the same time to control the position and pressure of the hydraulic cylinder separately. When the cylinder is extended, the position control of the cylinder is achieved by the signal u_1 of valve 1, and the pressure of rod chamber is controlled by the signal u_2 of valve 2. Since the pressure of the return chamber can be freely controlled during the running of the cylinder, the pressure value is usually set in a low range to reduce energy consumption. The process of cylinder retraction operates on the same principle.

The flow rate through servo valves can be expressed respectively as follows

$$Q_1 = C_d w x_{v1} \sqrt{\frac{2}{\rho} \Delta P_1} \quad (1)$$

$$Q_2 = C_d w x_{v2} \sqrt{\frac{2}{\rho} \Delta P_2} \quad (2)$$

where C_d and w are flow coefficient and area gradient of servo valve respectively. x_{vi} denotes the displacement of spool. ΔP_i is the pressure drop of the valve, expressed as

$$\Delta P_i = \begin{cases} P_s - P_i, & x_{vi} > 0 \\ P_i - P_r, & x_{vi} < 0 \end{cases}, i = 1, 2 \quad (3)$$

where P_s is the pump outlet pressure and P_r is the pressure of tank.

As the frequency response of the valve studied in this research is higher than actuator's, the servo valve can be considered as a proportional link that can be expressed as

$$x_v = k_s u \quad (4)$$

where k_s and u are valve gain and control signal of servo valve correspondingly.

Ignoring the external and internal leakage of cylinder, according to the flow continuity equation, we can get flow equations of the two chambers of cylinder respectively as follows

$$Q_1 = A_1 \frac{dx_p}{dt} + \frac{V_1}{\beta_e} \frac{dP_1}{dt} \quad (5)$$

$$Q_2 = A_2 \frac{dx_p}{dt} - \frac{V_2}{\beta_e} \frac{dP_2}{dt} \quad (6)$$

where β_e denotes oil effective bulk modulus, V_1 and V_2 are total volume of inlet chamber and return chamber of cylinder respectively.

The force balance equation of the system can be described by

$$P_1 A_1 - P_2 A_2 = m \frac{d^2 x_p}{dt^2} + F_{ext} \quad (7)$$

where x_p denotes the cylinder displacement, m means the effective mass of load, and F_{ext} is the sum of all loads on the cylinder including the viscous damping load, elastic loads, friction, etc.

For simplicity, let $k_v = C_d w \sqrt{2/\rho}$, then according to Eqs. (1) to (7), the mathematical model of IMEHSS can be

obtained as follows

$$\begin{cases} \ddot{x}_p = \frac{1}{m} (P_1 A_1 - P_2 A_2 - F_{ext}) \\ \dot{P}_1 = \frac{\beta_e}{V_1} (k_v k_s \sqrt{\Delta P_1} u_1 - A_1 x_p) \\ \dot{P}_2 = \frac{\beta_e}{V_2} (-k_v k_s \sqrt{\Delta P_2} u_2 + A_2 x_p) \end{cases} \quad (8)$$

Let $\mathbf{x} = [x_1 \ x_2 \ x_3 \ x_4]^T = [x_p \ \dot{x}_p \ P_1 \ P_2]^T$, the state space function of IMEHSS can be described as

$$\begin{cases} \dot{x}_1 = x_2 \\ \dot{x}_2 = \frac{1}{m} (x_3 A_1 - x_4 A_2 - F_{ext}) \\ \dot{x}_3 = \frac{\beta_e}{V_1} (k_v k_s \sqrt{\Delta P_1} u_1 - A_1 x_2) \\ \dot{x}_4 = \frac{\beta_e}{V_2} (-k_v k_s \sqrt{\Delta P_2} u_2 + A_2 x_2) \end{cases} \quad (9)$$

It can be noticed that IMEHSS is a multi-input multi-output system, with inputs being the control signals u_1 and u_2 of two servo valves, and outputs being the displacement x_p and the return pressure P_2 of the cylinder. The IMEHSS can be regarded as a pressure control subsystem and a position control subsystem. Although the hydraulic valve-controlled cylinder is decoupled mechanically in IMEHSS, and the displacement and pressure of hydraulic cylinder can be controlled separately, there is still a strong mechanical-hydraulic dynamic coupling between the two subsystems of displacement and pressure control.

III. DESIGN OF CONTROLLER

In order to achieve higher control accuracy of position tracking and pressure control of IMEHSS, an ADRC decoupling control method with online information compensation is proposed in this paper. Both internal and external disturbances of the system are treated as the total disturbance of the system in ADRC. And this total disturbance is extended to a system state variable that can be observed by the designed extended state observer (ESO). By compensating the total disturbance, to deal with the problem of nonlinearity and uncertainty of the system. The standard ADRC is composed of three parts: tracking differentiator (TD), ESO, and state error feedback (SEF) control law. TD is used for the acquisition of the derivative of signals and the configuration of transition processes. ESO is mainly used for the estimation of the total disturbance which is the core part of the ADRC controller. Since the estimation and compensation of the total disturbance is the core idea of ADRC, it is particularly important to accurately estimate the total disturbance by ESO. In order to reduce the burden on the observer and improve its state observation accuracy, the ESO is compensated in real time using online information. Thus, the amount of total disturbance that needs to be estimated is reduced. And the precision of position tracking and pressure control of cylinder can be improved.

The schematic diagram of ADRC controller studied in this paper is shown in Fig. 2.

A. POSITION CONTROL SYSTEM CONTROLLER DESIGN

The mathematical model of the position control subsystem can be obtained as follows

$$\begin{aligned} \ddot{x}_p = & \frac{\beta_e k_v k_s \sqrt{\Delta P_1} A_1}{V_1 m} u_1 - \frac{\beta_e A_1^2}{V_1 m} \dot{x}_p - \frac{F_{ext}}{m} \\ & + \frac{\beta_e k_v k_s \sqrt{\Delta P_2} A_2}{V_2 m} u_2 - \frac{\beta_e A_2^2}{V_2 m} \dot{x}_p + f_{ed} \end{aligned} \quad (10)$$

where f_{ed} is the unmodeled portion that causes the movement change of the cylinder including the external and internal leakage of the cylinder, friction force, etc.

As the position control subsystem requires at least three integrators from input u_1 to output x_p , the relative order of the position control system is three [13].

Let $d_d = -\frac{F_{ext}}{m} + \frac{\beta_e k_v k_s \sqrt{\Delta P_2} A_2}{V_2 m} u_2 - \frac{\beta_e A_2^2}{V_2 m} \dot{x}_p + f_{ed}$, $b_{o1} = \beta_e k_v k_s R_1 A_1 / V_1 m$, $a_1 = \beta_e k_v k_s (\sqrt{\Delta P_1} - R_1) A_1 / V_1 m$, $a_2 = -\beta_e A_1^2 / V_1 m$, and then Eq. (10) can be written as

$$\ddot{x}_p = b_{o1} u_1 + a_1 u_1 + a_2 \dot{x}_p + d_d \quad (11)$$

where R_1 is the normal value of pressure drop at servo valve.

Eq. (11) reveals that the first term on the right side of the equation is the cylinder dynamic change caused by the calculated flow rate of the nominal valve of pressure drop, the second term is the cylinder dynamic change caused by the deviation of nominal calculated flow rate from actual calculated flow rate, the third term is the cylinder dynamic change caused by the flow rate into the rodless chamber of the cylinder, and the fourth term is the cylinder dynamic change caused by the pressure control subsystem, the unmodeled part and the load disturbance. If the second to fourth terms are treated as the total disturbance, which is observed and compensated by ESO, it significantly increases the amount of total disturbance that the ESO needs to estimate. In order to reduce the amount of total disturbance, the second and third terms are compensated as the online information.

Let $f_d = a_1 u_1 + a_2 \dot{x}_p$, the Eq. (11) can be written as

$$\ddot{x}_p = b_{o1} u_1 + f_d + d_d \quad (12)$$

where d_d is the total disturbance, f_d is part of the online compensation information.

In order to make the tracking of the signal smoother and easier to tune, a linear tracking differentiator is adopted as follows [20], [21].

$$\begin{cases} \dot{v}_1 = v_2 \\ \dot{v}_2 = v_3 \\ \dot{v}_3 = v_4 \\ \dot{v}_4 = -\left[\omega_r^4 (v_1 - r) + 4\omega_r^3 v_2 + 6\omega_r^2 v_3 + 4\omega_r v_4 \right] \end{cases} \quad (13)$$

where v_1 denotes the tracking of reference signal r , v_2 denotes the differential of reference, v_3 denotes the second-order

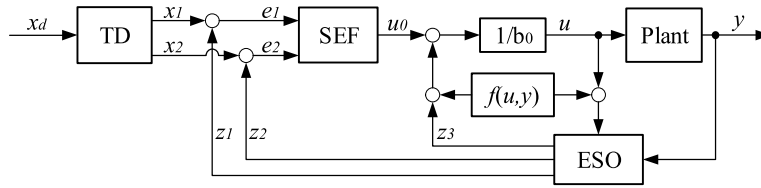


FIGURE 2. Schematic diagram of ADRC controller.

differential of reference, and ω_r is the tracking speed factor. The desired tracking effect is achieved by adjusting the value of ω_r .

Let $\mathbf{z} = [z_1 \ z_2 \ z_3 \ z_4]^T = [x_p \ \dot{x}_p \ \ddot{x}_p \ d_d]^T$, then Eq. (12) can be expressed as

$$\begin{cases} \dot{z}_1 = z_2 \\ \dot{z}_2 = z_3 \\ \dot{z}_3 = z_4 + b_{o1}u_1 + f_d \\ \dot{z}_4 = h \end{cases} \quad (14)$$

where $h = \dot{d}_d$.

To simplify the tuning process, and make it easier for engineers to understand and apply, a linear ADRC controller is used [22], [23], and [24].

Let \hat{z}_i as the estimation of z_i , then the designed ESO is

$$\begin{cases} \dot{\hat{z}}_1 = \hat{z}_2 - 4\omega_{o1}(\hat{z}_1 - z_1) \\ \dot{\hat{z}}_2 = \hat{z}_3 - 6\omega_{o1}^2(\hat{z}_1 - z_1) \\ \dot{\hat{z}}_3 = \hat{z}_4 + b_{o1}u_1 + f_d - 4\omega_{o1}^3(\hat{z}_1 - z_1) \\ \dot{\hat{z}}_4 = -\omega_{o1}^4(\hat{z}_1 - z_1) \end{cases} \quad (15)$$

where ω_{o1} is the bandwidth of ESO. By configuring the pole of ESO at the bandwidth ω_{o1} , the number of parameters to be tuned is reduced.

For simplicity, a linear SEF control law of PD-type is developed here.

$$\begin{cases} u_{01} = k_{o1}^3(r - \hat{z}_1) + 3k_{o1}^2(\dot{r} - \hat{z}_2) + 3k_{o1}(\ddot{r} - \hat{z}_3) \\ u_1 = (u_{01} - \hat{f}_d - \hat{d}_d)/b_{o1} \end{cases} \quad (16)$$

where r , \dot{r} and \ddot{r} are the reference, velocity and acceleration of the reference respectively. They can be obtained by the tracking differentiator. k_{o1} is the bandwidth of SEF, and tracking errors of displacement can be changed by adjusting the value of k_{o1} .

B. PRESSURE CONTROL SYSTEM CONTROLLER DESIGN

Since the flow rate of servo valve is determined by the speed of cylinder, and according to Eqs. (2) and (4), when the flow rate is constant, the control signal of servo valve is inversely proportional to the return pressure of the chamber, therefore, the pressure control subsystem of IMEHSS is passive.

According to the block diagram of IMEHSS, the pressure control goes through at least one integrator from input u_2 to output P_2 , so the first-order system is used for the pressure control subsystem.

According to Eqs. (2) and (6), the mathematical equation of the pressure control subsystem is

$$\dot{P}_2 = \frac{-\beta_e k_v k_s \sqrt{\Delta P_2}}{V_2} u_2 + \frac{A_2 \beta_e}{V_2} \dot{x}_p + f_{ep} \quad (17)$$

where f_{ep} is the pressure change caused by unmodeled part and position control system, including internal and external leakage of the cylinder.

In order to reduce the burden of the controller and ESO of the pressure control subsystem and to improve the estimation accuracy of the observer, the controller with information compensation system is used.

Let $b_{o2} = -\beta_e k_v k_s R_2 / V_2$, $a_3 = A_2 \beta_e / V_2$, $d_p = -\beta_e k_v k_s (\sqrt{\Delta P_2} - R_2) / V_2 + f_{ep}$, then Eq. (17) can be written as

$$\dot{P}_2 = b_{o2}u_2 + f_p + d_p \quad (18)$$

where $f_p = a_3 \dot{x}_p$ is the pressure change in return chamber due to the cylinder velocity.

As f_p has a large impact on the return chamber pressure, considering it as a total disturbance significantly increases the amount of the total disturbance, as well as increase the burden on the ESO. Therefore, this component is compensated to the controller as online information compensation. Then d_p is the total disturbance of pressure control subsystem. And the speed of the cylinder \dot{x}_p can be obtained from a tracking differentiator for the displacement of the cylinder.

Let $\theta = [\theta_1 \ \theta_2]^T = [P_2 \ d_p]^T$, then the state-space function of pressure control subsystem can be expressed as follows

$$\begin{cases} \dot{\theta}_1 = b_{o2}u_2 + f_p + \theta_2 \\ \dot{\theta}_2 = g \end{cases} \quad (19)$$

where, $g = \dot{d}_p$.

The ESO with compensation information is designed according to Eq. (19) as follows

$$\begin{cases} \dot{\hat{\theta}}_1 = \hat{\theta}_2 + 2\omega_{o2}(\hat{\theta}_1 - \theta_1) + b_{o2}u_2 + f_p \\ \dot{\hat{\theta}}_2 = -\omega_{o2}^2(\hat{\theta}_1 - \theta_1) \end{cases} \quad (20)$$

where ω_{o2} is the bandwidth of ESO of pressure control system, and $\hat{\theta}_i$ is the estimation of θ_i .

A PD-type linear SEF control law with online compensation information is developed for the pressure control subsystem.

$$\begin{cases} u_{o2} = k_{o2}(r - z_1) \\ u_2 = (u_{o2} - \hat{d}_d - \hat{f}_p)/b_{o2} \end{cases} \quad (21)$$

where, k_{o2} is the adjusted parameter.

During the process of parameter tuning, the displacement control system and the pressure control system can be adjusted separately. Taking the extension of hydraulic cylinder as an example, when tuning the parameters of the position control system, set the input signal u_2 of valve 2 to a constant value, and gradually increase ω_{o1} until the curve of cylinder displacement observed by ESO is the same as the curve of the actual cylinder displacement. Then regulate k_{o1} , so that the system displacement tracking accuracy reaches a satisfactory result. And the regulation of the parameter k_{o1} will not affect the results of ESO. The method of tuning the parameters of pressure control system is the same. From the process of tuning parameters, it can be found that the position and pressure control subsystems decoupled.

IV. SIMULATIONS AND EXPERIMENTS VERIFICATION

In this section, the results of co-simulations and experiments are given. Ramp tracking of cylinder position tests are performed for both simulation and experiment. The slope of the ramp signal is 0.7 m/s and the amplitude is 0.25 m. The pressure of return chamber is controlled at 10 bar.

A. CO-SIMULATION

In this research, simulations were done by AMESim and MATLAB/Simulink. The hydraulic system of IMEHSS was set up in AMESim that takes into account system friction, oil leakage and compression. The controller was built in MATLAB/Simulink. The parameters used in the simulation of hydraulic system are shown in Table 1. According to Section II, it is known that IMEHSS is characterized by nonlinearity and time-varying parameters. Since ADRC is designed based on the concept of total perturbation, fixed parameters can be used instead of variable parameters, and the errors of parameter modeling can be treated as disturbance, which can be observed and compensated by ESO. Table 2 shows parameters that are set in the simulation model.

TABLE 1. Hydraulic system simulation parameters.

Parameter	Value
Displacement of pump (ml/r)	50
Motor speed (r/min)	1500
Pressure of pump (bar)	70
Maximum flow of valve (L/min)	100
Cylinder piston diameter (m)	0.063
Rod diameter (m)	0.045
Cylinder stroke (m)	0.5
Mass (Kg)	100
Friction (N)	100

Firstly, the cylinder extension simulation experiment is carried out. The nominal values are calculated according to the parameters in Table 2 as, $b_{o1} = 896.74$, $b_{o2} = -306.29$. The parameters $\omega_{o1} = 12$, $k_{o1} = 10$, $\omega_{o2} = 60$, $k_{o2} = 80$, are selected, and the nominal values calculated for the

TABLE 2. Controller simulation parameter.

Parameter	Value
k_v	16.9
k_s	0.025
R_1	5.916
R_2	3.162

compensation information parameters are, $a_{o1} = 179.35$, $a_{o2} = 7.94 \times 10^4$, $a_{o3} = 2.10 \times 10^4$, for simulation. Adjust PID controller parameters of the position control subsystem to improve its tracking accuracy as much as possible without overshooting, and the parameters are set to P = 500, I = 5, D = 0. Since the pressure control system is passive, when the flow rate is constant, the control signal of servo valve is inversely proportional to the pressure of return chamber. However, in PID control, the control signal is proportional to the deviation, so traditional PID can't be directly applied in the pressure control system. Therefore, the PID controller of pressure control system in this paper takes the form of

$$u_2 = 1/(k_p e + k_d \int edt) \tag{22}$$

where k_p is the coefficient of the proportional term and k_d is the coefficient of the integral term. Obviously, it increases the difficulty of parameter adjustment. The parameters $k_p = 0.07$, $k_d = 0.3$ are set by trial and error.

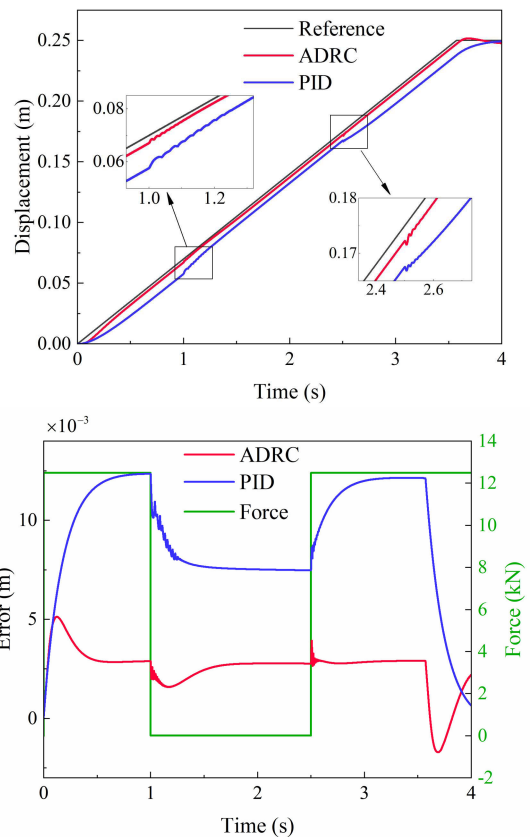


FIGURE 3. Cylinder extension position control with load disturbance.

To test the performance of disturbance rejection of the controller for load, the load disturbance is added during cylinder operation. During cylinder extension, a 4MPa pressure is exerted to the loading cylinder at the beginning, then, it is released at 1s, and reloaded at 2.5s.

Fig. 3 to Fig. 6 show the simulation results of cylinder extension with load disturbance. From Fig. 3, it obvious that the tracking errors of ADRC are significantly smaller than that of PID in the position control subsystem, and the tracking errors don't change significantly after the load disturbance. The tracking errors of PID change greatly when the load changes. when there is a load, the tracking errors of PID are about 12mm, and when there is no load, they are about 7.5mm. The ADRC tracking errors are maintained at about 3 mm after small fluctuations occur during load disturbances. This is due to the fact that the load disturbances are estimated and compensated in the ADRC controller. The results of simulation show that ADRC performs better than PID in resisting load disturbances.

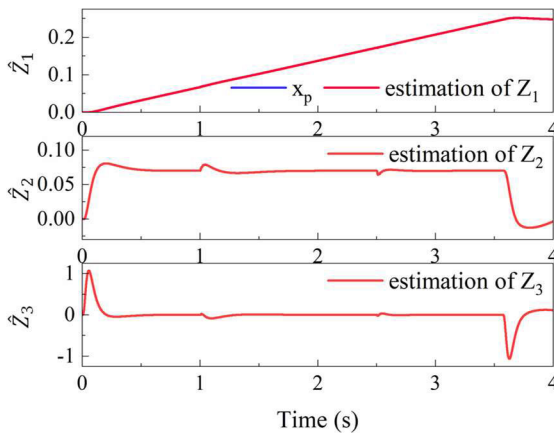


FIGURE 4. State estimated by ESO during cylinder extension with load disturbance.

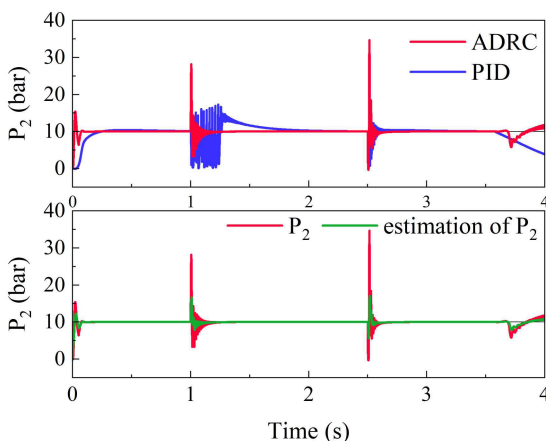


FIGURE 5. Cylinder extension pressure control with load disturbance.

Fig. 4 shows the state values of displacement, velocity and acceleration of cylinder estimated by ESO during the cylinder extension process. It can be also seen that the displacement

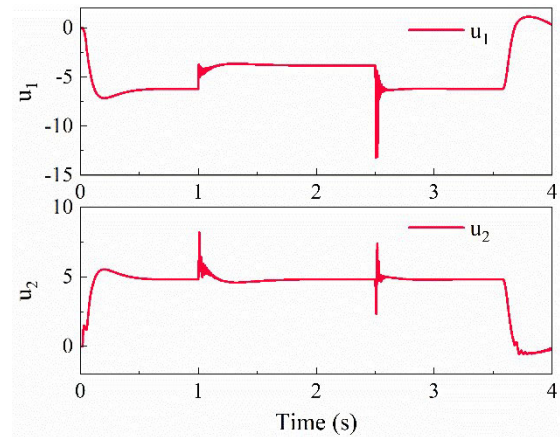


FIGURE 6. Control signal during cylinder extension with load disturbance.

estimated by ESO and the actual displacement of the cylinder completely coincide with each other, indicating that ESO achieves a very good observation effect.

Fig. 5 shows the pressure control curves of the rod chamber of the cylinder with load disturbance during cylinder extension. As can be seen from Fig. 5, the regulation time of ADRC is significantly shorter than that of PID in the initial stage of cylinder running. The tuning time of ADRC is also shorter than PID when affected by load disturbances. From Fig. 5, it can be shown that the pressure estimated and the pressure P2 of rod chamber are basically the same, indicating that the state observation accuracy of ESO compensated by online information is high.

Fig. 6 shows the control signals output from the controller during the cylinder extension with load disturbance. The position control signal is u_1 , and the pressure control signal is u_2 . From Fig. 6, it can be seen that in the process of load disturbance injection, the control signals change accordingly to reduce the impact on the system due to the load disturbance. Due to the disappearance of the load at 1 s, the pressure of the rodless chamber decreases. In order to keep the flow rate constant under the constant supply pressure, it is necessary to reduce the opening of valve to maintain a constant pressure drop at the valve port. Therefore, the absolute value of u_1 is smaller when there is no load, and its absolute value is larger when there is a load.

Then the cylinder retraction simulation test is carried out. The nominal values are calculated according to the parameters in Table 2. The values and meanings of parameters for simulation are shown in Table 3. Parameters of PID controller of position control system were set to $P = 230$, $I = 5$, $D = 0$, and the pressure control system used the same inverse proportional control as the cylinder extension, which parameters are set to $k_p = 0.01$, $k_d = 0.1$.

During cylinder retraction, the load disturbance is applied too. During cylinder retraction, apply a 3 MPa pressure to the loading cylinder at beginning, then, it is released at 1s, and reloaded at 2.5 s. Fig. 7 to Fig. 9 show the simulation results of cylinder retraction with load disturbance. From Fig. 7,

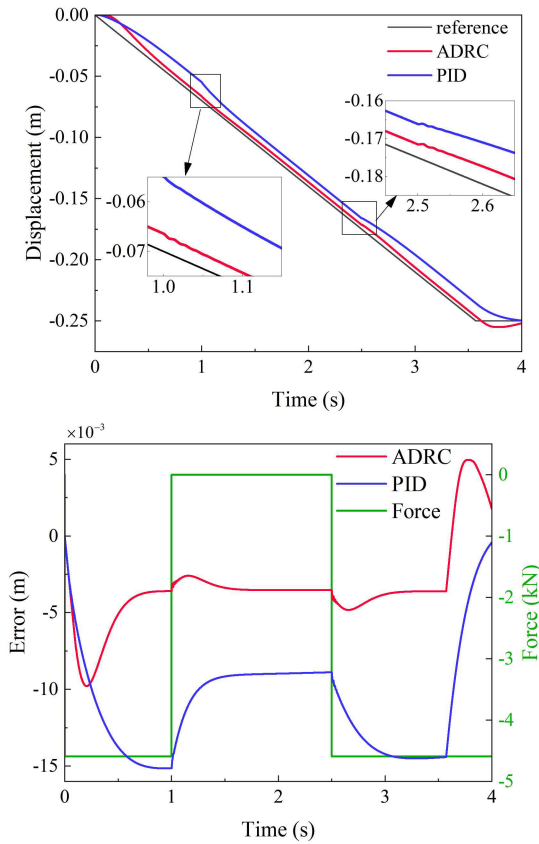


FIGURE 7. Cylinder retraction position control curves with load disturbance.

TABLE 3. Values and meanings of parameters for cylinder retraction simulation.

Parameter	Meaning	Value	
Position control system	b_{i1}	gain of input signal	739.43
	ω_{i1}	bandwidth of ESO	12
	k_{i1}	bandwidth of control	10
	a_{i1}	compensation coefficient of input signal	147.89
Pressure control system	a_{i2}	compensation coefficient of velocity	3.21e4
	b_{i2}	gain of input signal	-181.94
	ω_{i2}	bandwidth of ESO	60
	k_{i2}	bandwidth of control	80
	a_{i3}	compensation coefficient of pressure control	2.55e4

it can be found that tracking errors of ADRC are significantly smaller than PID. When the load changes, the tracking errors of ADRC are basically unchanged at about -3.5 mm, but tracking errors of PID are more variable and highly related to the load. When the load is larger, the tracking errors are larger about -14.5 mm, when the load is smaller, the tracking errors become smaller about -9 mm, which is basically the consistent with the process of cylinder extending. This

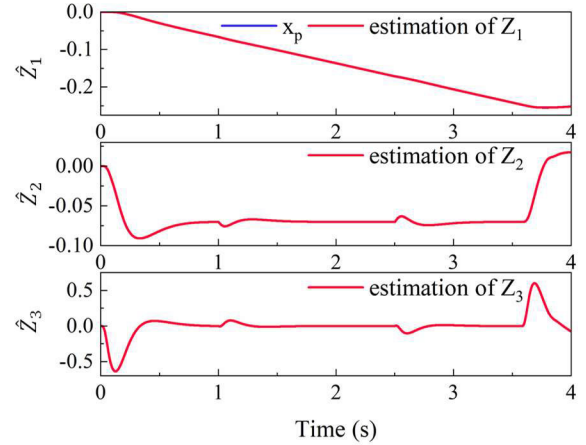


FIGURE 8. State estimated by ESO during cylinder retraction with load disturbance.

indicates that the ADRC controller has stronger ability to resist load interference.

Fig. 8 shows the state estimated by ESO during cylinder retraction with load disturbance. It can be also seen that the displacement estimated by ESO and the actual displacement of the cylinder completely coincide with each other, indicating that ESO achieves a very good observation effect during cylinder retraction.

Fig. 10 shows the pressure control curves of rodless chamber of cylinder with load disturbance during cylinder retraction. As can be found in the figure, the pressure of ADRC controller quickly reaches the target value of 10 bar after a small overshoot in the initial stage of cylinder operation, and the regulation time is significantly shorter than that of PID. And the accuracy of the pressure estimates is high.

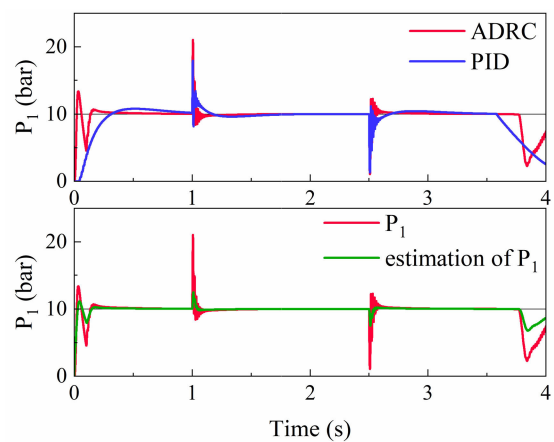


FIGURE 9. Cylinder retraction pressure control with load disturbance.

By comparing Fig. 5 and Fig. 9, it can be found that the results of pressure controlled by ADRC controller are nearly unchanged during the process of cylinder extension and retraction, while it is very different for PID controller. This is because the pressure control system is passive pressure

control, when the speed of the cylinder is constant, the rodless chamber is return chamber and the oil flow rate is small during cylinder extends, while the flow rate of oil is large during cylinder retracts as the return chamber is the rod chamber. So, the PID controller is more effective in controlling the pressure during cylinder retraction than cylinder extension. However, for the ADRC controller, the results of pressure control are almost the same during the cylinder extension and cylinder retraction, which indicates that the ADRC controller has good robustness for different working conditions.

Fig. 10 shows the control signals output from the controller during the cylinder retraction with load disturbance. The control signals are opposite to cylinder extension, u_1 is the pressure control signal and u_2 is the position control signal. When there is load interference, the control signals respond immediately. And the value of u_2 is smaller when there is no load, and it is larger when there is a load.

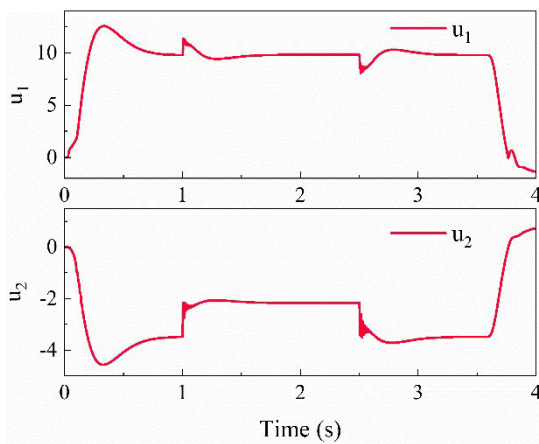


FIGURE 10. Control signal during cylinder retraction with load disturbance.

In order to further quantitatively analyze and compare the simulation results, the Absolute Peak Error (APE) I_{APE} and Root Mean Square Error (RMSE) I_{RMSE} are used as the evaluation criteria respectively. I_{APE} and I_{RMSE} are defined as follows

$$I_{APE} = \max_{i=1,2,\dots,n} (|e_i|) \quad (23)$$

$$I_{RMSE} = \sqrt{\frac{\sum_{i=1}^n e^2}{n}} \quad (24)$$

The numerical evaluation indexes of cylinder extension and retraction in the simulation experiments are shown in Table 4.

TABLE 4. Simulation result indicators.

	cylinder extension		cylinder retraction	
ADRC	$I_{APE}=5.0e-3$	$I_{RMSE}=2.8e-3$	$I_{APE}=9.8e-3$	$I_{RMSE}=4.3e-3$
PID	$I_{APE}=1.2e-2$	$I_{RMSE}=9.5e-3$	$I_{APE}=1.5e-2$	$I_{RMSE}=1.1e-2$

From Table 4, it can be seen that the performance of the method proposed in this paper is better. Compared with the classical PID, the proposed method can reduce the APE by 58.3% and the RMSE by 70.5% during cylinder extension; during cylinder retraction, the APE is reduced by 34.7% and the RMSE is reduced by 60.9%.

B. EXPERIMENTAL VERIFICATION

In order to further verify the reliability of the method proposed, experiments are carried out on the test rig. Fig. 11 shows the photo and principle of test rig. The control system of the test rig is composed of industrial control computer, digital processor, data acquisition system which including displacement and pressure sensors. And the sampling frequency of the system is 1000 Hz. On the host computer, the ADRC model established in Simulink software is transformed into c language by Control-Desk software, and the human-computer interaction interface required by the experiment is established.

TABLE 5. Main components of experiment platform.

Element	Type	Quantity
Pump	A4VSO71HD1/10R	1
Motor	EO1220F203R40YOKB1-TF	1
Valve	4ERPEH10C4B100L-3X/M	2
dSPACE	MicroLabBox	1
Cylinder	SY-63-45-500	2

For the IMEHS system, the rodless and rodded chambers of the test cylinder are controlled by separate servo direction valves, and different loads are simulated to be loaded to the test cylinder by the loading cylinder. The system flow rate can be controlled by the pump’s displacement control device and motor speed. Table 5 shows the main components of the experiment platform.

First, the cylinder extension test without load disturbance is carried out, and the displacement and tracking errors of the cylinder are shown in Fig. 12. The parameters values of the cylinder extension experiment are the same as those of simulation. As can be seen from Fig. 12, tracking errors of ADRC are smaller than that of PID, and the estimation of the cylinder displacement by ADRC is generally consistent with the actual displacement of the cylinder, indicating that the observer has good performance and can accurately observe the cylinder displacement in real time. Fig. 13 shows the curves of the observed values of ESO for cylinder displacement and velocity and acceleration in the cylinder extension experiment. Comparing Fig. 12 Fig. 13 and Fig. 3 Fig. 4, it can be found that the results of simulation and test are generally the same in the stable operation stage of the cylinder, which indicates that the simulation model and the test bench have a high degree of matching, and the simulation results have certain reference value and credibility. The results of simulations and experiments show small differences which is due to some differences between the simulation model and the actual test bench that may

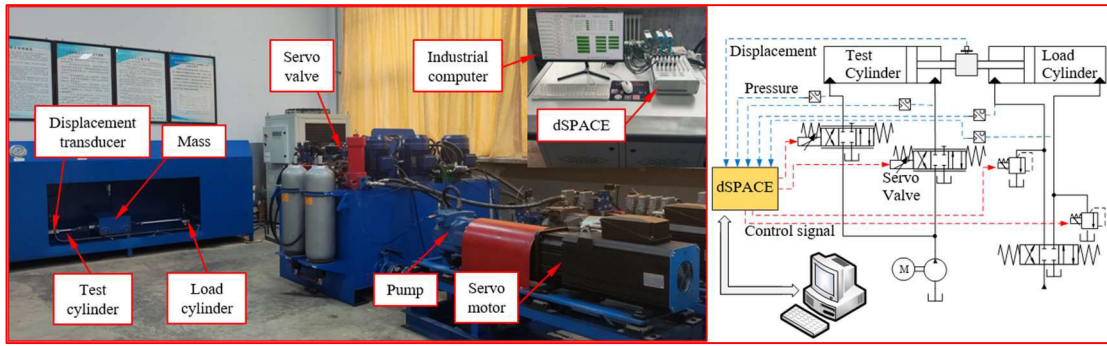


FIGURE 11. Photo and principle of test rig.

be caused by friction model errors, test bench installation accuracy, etc.

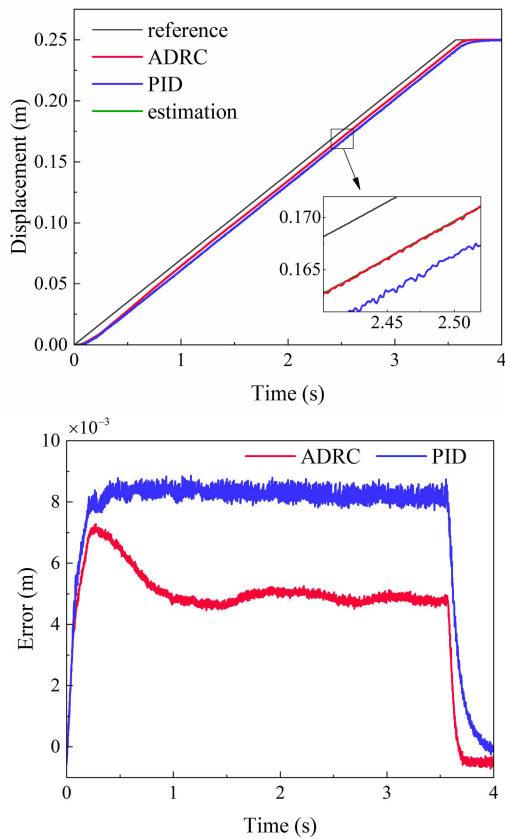


FIGURE 12. Results of position control of cylinder extension experiment without load disturbance.

Fig. 14 shows the compensation information and disturbance observed curves during the cylinder extension process. The curves are relatively smooth because there is no load disturbance during the cylinder operation.

Fig. 15 shows the pressure of return chamber during cylinder extension without load condition. As can be seen from the graph, the pressure controlled by ADRC is significantly better than that of PID, which is basically stabilized at 10 bar. The pressure estimate has a certain error in the initial stage, and after about 0.5 s, the pressure

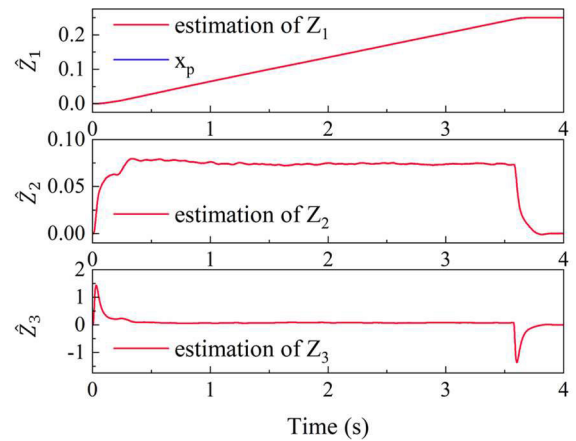


FIGURE 13. Results of state estimated by ESO of cylinder extension without load disturbance.

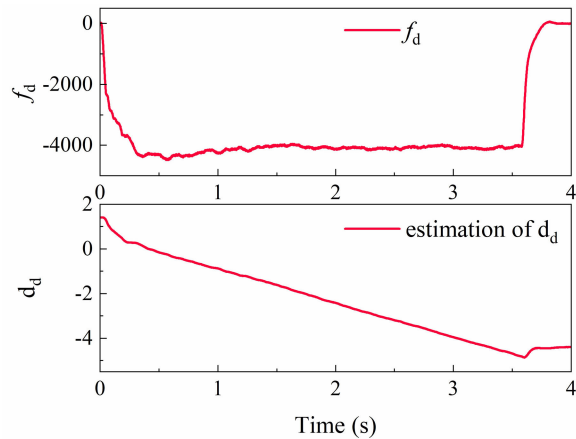


FIGURE 14. Disturbance and compensation information of position control system of cylinder extension without load disturbance.

estimated values are the same as the actual values, and have high observation accuracy. Fig. 16 shows the pressure control compensation information and disturbance curves. Because the cylinder runs relatively smoothly, and there is no load interference, so the curves are relatively smooth.

Secondly, the cylinder extension test with load disturbance is carried out. During the cylinder extension process, a load pressure of 4 MPa is first applied to the rodless chamber of

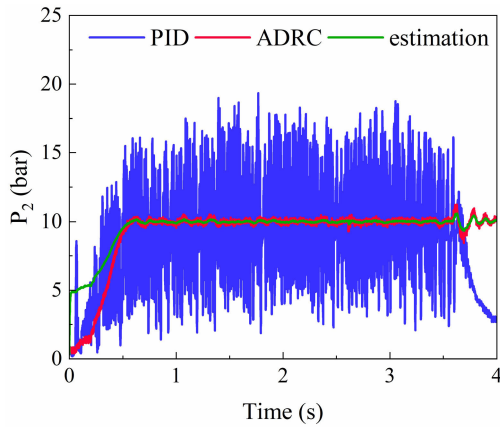


FIGURE 15. Results of pressure control of cylinder extension experiment without load disturbance.

the load cylinder, and it is removed at 1.5 s. Fig. 17 shows the curves of position control of cylinder extension with load disturbance. From Fig. 17, it can be noticed that tracking errors of displacement of ADRC vary relatively small under the condition of load disturbance, but the displacement tracking errors of PID change rather large, which indicates that the ADRC is more resistant to disturbances. Comparing Fig. 3 and Fig. 17, it can be noticed that the results of simulations and experiments are basically the same, indicating that the simulation model has high credibility and the simulation results have reference value.

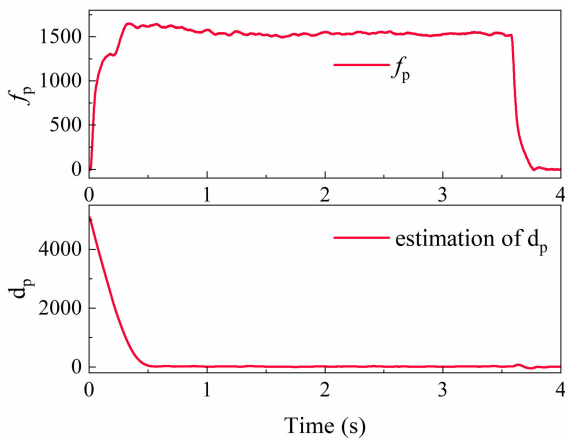


FIGURE 16. Disturbance and compensation information of pressure control system of cylinder extension without load disturbance.

Fig. 18 shows the estimations of displacement, velocity and acceleration during cylinder extension with load disturbance. Comparison of Fig. 18 and Fig. 13 shows that when the cylinder is disturbed by the load, there are corresponding changes in the observed cylinder velocity and acceleration. At 1.5 s, the velocity and acceleration curves of the cylinder fluctuate slightly due to the change in load. Comparing Fig. 18 and Fig. 4, it can be found that the simulation results are the same as the experimental results.

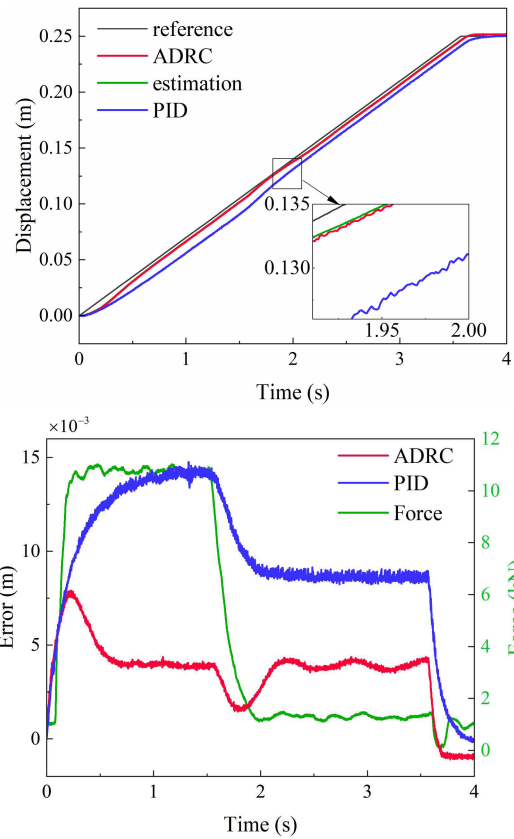


FIGURE 17. Results of position control of cylinder extension experiment with load disturbance.

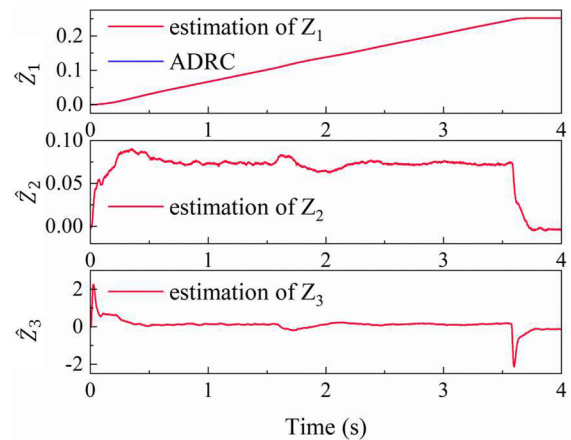


FIGURE 18. Results of state estimated by ESO of cylinder extension with load disturbance.

Fig. 19 shows the disturbance and compensation information of position control system of cylinder extension with load disturbance. From the figure, it can be found that when the cylinder is subjected to different load forces, the compensation information and disturbance observed will change accordingly to compensate the controller and make the cylinder operate stably. Comparing Fig. 14 and Fig. 19, it can also be found that the compensation information and the disturbance observation values are the same when

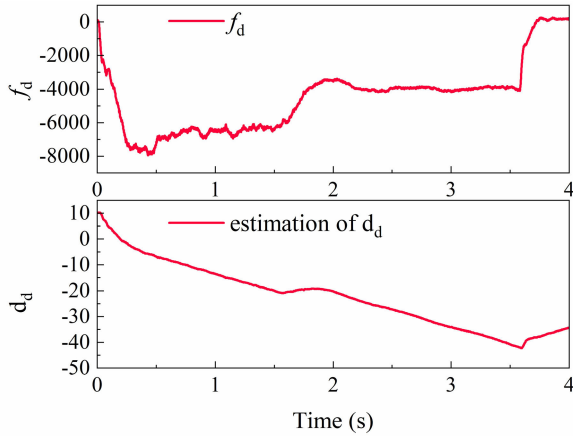


FIGURE 19. Disturbance and compensation information of position control system of cylinder extension with load disturbance.

the cylinder operates without load, and the compensation information is larger when it operates with load. When the load changes, the load disturbance estimated will change to suppress the fluctuation of the cylinder. Thus, it is shown that information compensation and interference observation play an important role during cylinder operation.

Fig. 20 shows the results of pressure control of cylinder extension experiment with load disturbance. As can be seen from the graph, the pressure control of ADRC is more accurate. Fig. 21 shows disturbance and compensation information of pressure control system of cylinder extension without load disturbance. From Fig. 21, it can be noticed that both the compensation information and the estimated disturbance change when the cylinder is subjected to a load change. Comparison of Fig. 16 and Fig. 21 shows that the results are the same under the no-load condition, but when the load changes, the compensation information and estimated disturbance change to compensate the system and serve to suppress the interference. It is illustrated that in the pressure control system, the disturbance observed by ESO is more accurate, and the ADRC controller can realize the observation and compensation of disturbance with anti-interference capability.

Fig. 22 is the control signals of cylinder extension experiment with load disturbance. The input signal of the servo valve is a voltage signal of 0-10 V. From the figure, it can be seen that the position control signal u_1 has a larger value when the load is larger. At the moment of load unloading, the velocity of the cylinder becomes larger, there is a tendency to accelerate. At this time, the return chamber pressure becomes larger, in order to keep the pressure unchanged, it is necessary to increase the valve opening so that the output flow rate of valve can be increased. Therefore, when the load is unloaded, the pressure control signal curve u_2 has a downward fluctuation.

Then, the experiment of cylinder retraction with load disturbance is carried out. During cylinder retraction, a pressure of 3 MPa is first applied to the rod chamber of the

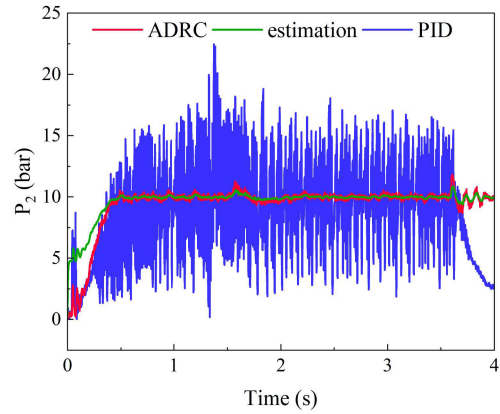


FIGURE 20. Results of pressure control of cylinder extension experiment with load disturbance.

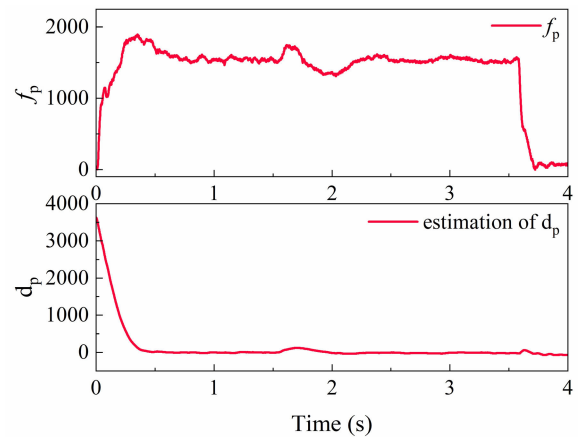


FIGURE 21. Disturbance and compensation information of pressure control system of cylinder extension with load disturbance.

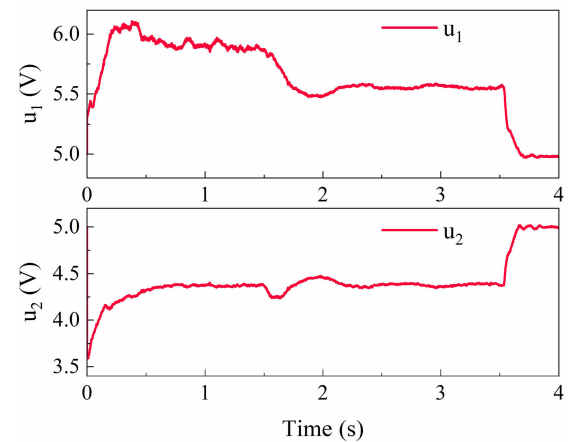


FIGURE 22. Cylinder extension control signals under load disturbance conditions.

loading cylinder, and this pressure is released at 1.5 s. The values of experimental parameters are the same as the simulation parameters. The experimental results are shown in Fig. 23 to Fig. 27. Fig. 23 shows the position control curves of cylinder retraction with load disturbance. From

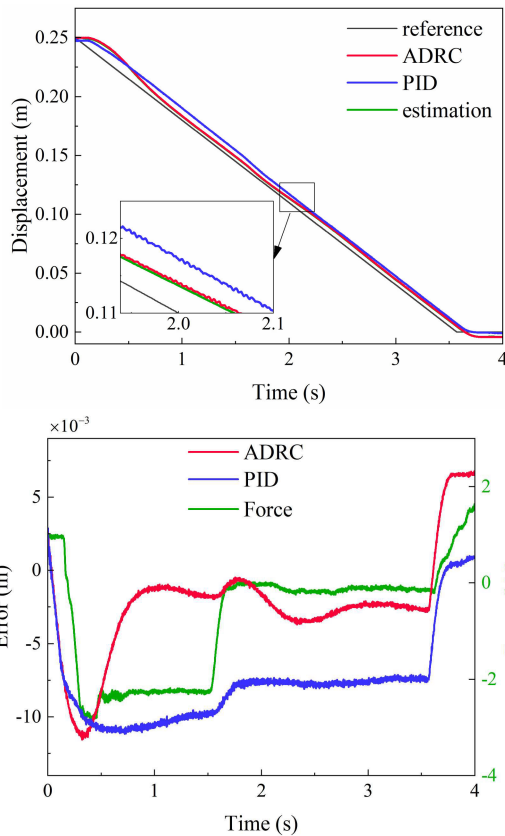


FIGURE 23. Results of position control of cylinder retraction experiment with load disturbance.

Fig. 23, it can be noticed that tracking errors of ADRC are significantly lower than those of PID, and that the tracking errors of ADRC are essentially unchanged when the load change occurs, whereas the PID undergoes a large change. Fig. 24 shows the observed curves of displacement velocity and acceleration of the cylinder when the load is changed during the cylinder operation. The simulation and experiment results are basically consistent as can be seen in Fig. 8 and Fig. 24. Fig. 25 shows the experimental results of disturbance and compensation information of position control system of cylinder retraction with load disturbance.

Fig. 26 shows the results of pressure control of cylinder retraction experiment with load disturbance. As can be seen from the figure, there is a slight overshoot of the pressure control of ADRC in the initial state, and there is a small fluctuation when the load changes, but the ADRC control accuracy is higher than PID in the whole pressure control process. Comparison of Fig. 15 Fig. 20 and Fig. 26 reveals that the pressure control accuracy of PID during cylinder retraction is higher than that of cylinder extension. As mentioned, this is due to the fact that when the cylinder speed is fixed, the flow rate of the rodless chamber is larger than that of the rodded chamber, and in passive pressure control, the pressure is easier to achieve control with a larger flow rate. This indicates that the pressure control robustness of ADRC is good.

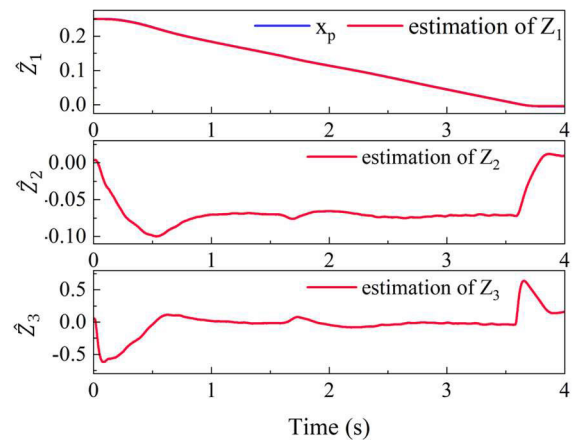


FIGURE 24. Results of state estimated by ESO of cylinder retraction with load disturbance.

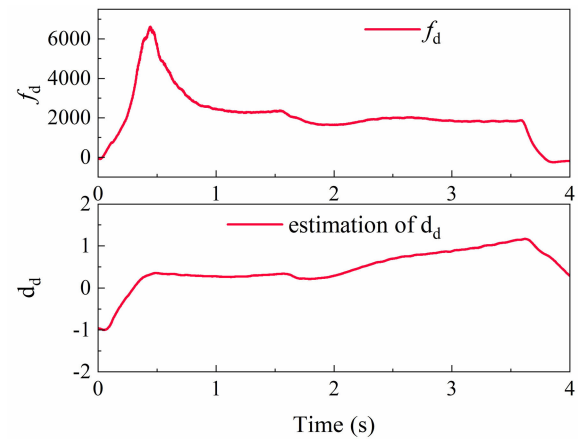


FIGURE 25. Disturbance and compensation information of position control system of cylinder retraction with load disturbance.

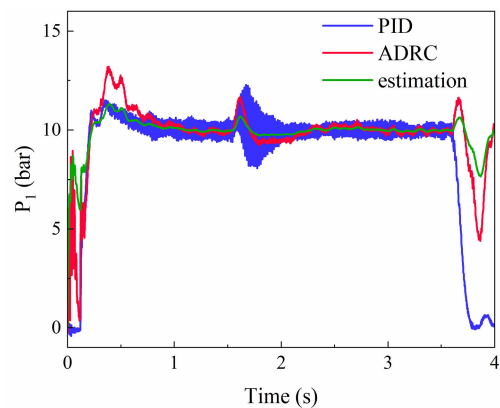


FIGURE 26. Results of pressure control of cylinder retraction experiment with load disturbance.

Fig. 27 shows the disturbance and compensation information of pressure control system, which changes to suppress the effect of disturbance on the system when the load changes.

Fig. 28 shows the output signals of the controller during cylinder retraction under the load disturbance condition. And u_2 is the position control signal. As the rod chamber is the

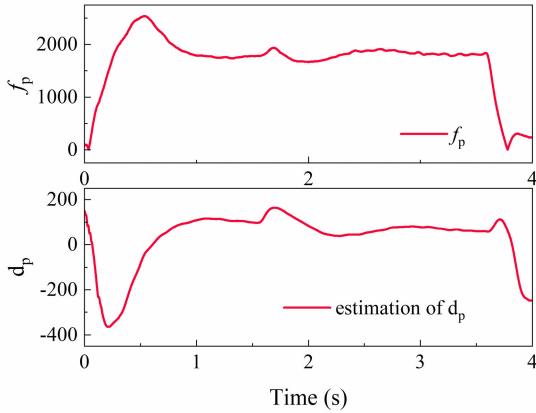


FIGURE 27. Disturbance and compensation information of pressure control system of cylinder retraction with load disturbance.

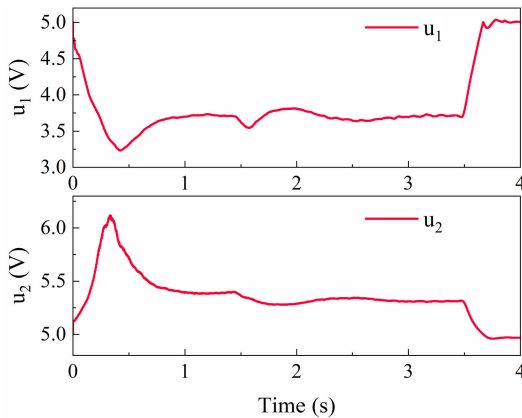


FIGURE 28. Cylinder retraction control signals under load disturbance conditions.

inlet chamber during cylinder retraction, the flow rate of cylinder is small when the velocity is constant. Comparing Fig. 22 and Fig. 28, it can be found that the position control signal u_2 in Fig. 28 is smaller than the position control signal u_1 in Fig. 22.

The numerical evaluation indexes of cylinder extension and retraction in experiments with load disturbance are shown in Table 6.

TABLE 6. Indicators of test results.

	cylinder extension		cylinder retraction	
ADRC	$I_{APE}=7.9e-3$	$I_{RMSE}=4.0e-3$	$I_{APE}=1.1e-2$	$I_{RMSE}=4.3e-3$
PID	$I_{APE}=1.5e-2$	$I_{RMSE}=1.0e-2$	$I_{APE}=1.1e-2$	$I_{RMSE}=8.2e-3$

As can be seen from Table 6, during cylinder extension with load disturbance, ADRC reduces the APE by 47.3% and the RMSE by 60% compared to PID. During cylinder recovery, the APE ADRC is the same as PID, but the RMSE is reduced by 47.6%.

V. CONCLUSION

In this paper, an online information compensation ADRC decoupling control method is proposed for the problems

of strong coupling of pressure and position subsystems, complex operating conditions, large load interference, and time-varying system parameters of IMEHSS. The rationality, effectiveness and practicality of the method are verified by simulations and experiments. According to the results of simulations and experiments, the following conclusions can be obtained.

(1) This method enables decoupling of position and pressure control subsystems of IMEHSS, and can realize that the pressure and position control systems can adjust the parameters separately. By compensating the online information for ESO, the burden of the observer can be reduced, which can improve the tracking accuracy of position control subsystem and the pressure control accuracy of the return chamber.

(2) By comparing with the results of PID, it is found that the method proposed has strong anti-interference ability against load disturbance, and the position tracking accuracy and pressure control accuracy are high. Simulation results show that the proposed method reduces the RMSE by more than 60%, and the experimental results show that the proposed method results in a reduction of the RMSE of the cylinder tracking error by about 47%.

(3) This method can realize that the parameters regulated of the passive pressure control subsystem are proportional to the control signal which eases the parameters tuning process. This method does not strictly depend on the mathematical model of the system, and the parameters adjustment are facilitated which is easier for engineers to understand and apply, and has strong practicability which is convenient for promotion and application.

In the further work, the authors will investigate the effect of the tracking differentiator on the controller performance. And the method proposed in this paper is compared with more advanced algorithms to verify the generality and applicability of the algorithm.

APPENDIX

The stability proof of the controller is given below. Take the cylinder extension as an example. For position control subsystem.

Let \tilde{e} as the state estimation error of ESO. Based on the analysis above, the state error equation of ESO can be obtained from Eqs. (14) and (15) as follows

$$\dot{\tilde{e}} = (A - Lc) \tilde{e} + Eh \tag{25}$$

where

$$A - Lc = \begin{bmatrix} -l_1 & 1 & 0 & 0 \\ -l_2 & 0 & 1 & 0 \\ -l_3 & 0 & 0 & 1 \\ -l_4 & 0 & 0 & 0 \end{bmatrix},$$

$$E = \begin{bmatrix} 0 \\ 0 \\ 0 \\ 1 \end{bmatrix}, \quad \begin{bmatrix} l_1 \\ l_2 \\ l_3 \\ l_4 \end{bmatrix} = \begin{bmatrix} 4\omega_o \\ 6\omega_o^2 \\ 4\omega_o^3 \\ \omega_o^4 \end{bmatrix}.$$

For analysis, coordinate transformations are performed.

Let $\varepsilon_i = \frac{\tilde{e}_i}{\omega_o^{i-1}}$, $i = 1, 2, 3, 4$. Then the Eq. (26) can be obtained as follows

$$\dot{\varepsilon}(t) = \omega_o A_\varepsilon \varepsilon + E \frac{h}{\omega_o^3} \quad (26)$$

where

$$A_\varepsilon = \begin{bmatrix} -4 & 1 & 0 & 0 \\ -6 & 0 & 1 & 0 \\ -4 & 0 & 0 & 1 \\ -1 & 0 & 0 & 0 \end{bmatrix}.$$

Solving Eq. (26), the solution of $\varepsilon(t)$ can be expressed as follows

$$\varepsilon(t) = e^{\omega_o A_\varepsilon t} \varepsilon(0) + \int_0^t \frac{Eh}{\omega_o^3} e^{\omega_o A_\varepsilon (t-\tau)} d\tau \quad (27)$$

As A_ε is Hurwitz, there exists a finite time $T_1 > 0$, such that

$$|e^{\omega_o A_\varepsilon t}|_{ij} \leq \frac{1}{\omega_o^4} \quad (28)$$

Let

$$e^{\omega_o A_\varepsilon t} = \begin{bmatrix} a_{11} & a_{12} & a_{13} & a_{14} \\ a_{21} & a_{22} & a_{23} & a_{24} \\ a_{31} & a_{32} & a_{33} & a_{34} \\ a_{41} & a_{42} & a_{43} & a_{44} \end{bmatrix}$$

and

$$\varepsilon_{sum}(0) = |\varepsilon_1(0)| + |\varepsilon_2(0)| + |\varepsilon_3(0)| + |\varepsilon_4(0)|$$

Then

$$\begin{aligned} & \left| \left[e^{\omega_o A_\varepsilon t} \varepsilon(0) \right]_{i=1,2,3,4} \right| \\ &= |a_{i1}\varepsilon_1(0) + a_{i2}\varepsilon_2(0) + a_{i3}\varepsilon_3(0) + a_{i4}\varepsilon_4(0)|_i \\ &\leq \frac{1}{\omega_o^4} (|\varepsilon_1(0)| + |\varepsilon_2(0)| + |\varepsilon_3(0)| + |\varepsilon_4(0)|) \\ &= \frac{\varepsilon_{sum}(0)}{\omega_o^4} \end{aligned} \quad (29)$$

In this research the main disturbances in hydraulic system studied in the paper are parameters variations and load disturbances. In practical engineering, none of these disturbance changes are instantaneous, so it is reasonable to assume that the rate of disturbance change is bounded. Therefore, the disturbance is considered to satisfy the Lipschitz continuity. As $h \dot{=} d$, assuming $|h| < \delta$, that is, h is a bounded quantity.

Let $p(t) = \int_0^t \frac{Eh}{\omega_o^3} e^{\omega_o A_\varepsilon (t-\tau)} E \frac{h}{\omega_o^3} d\tau$, then

$$\begin{aligned} |p(t)|_{i=1,2,3,4} &\leq \frac{\delta}{\omega_o^4} \int_0^t \left[e^{\omega_o A_\varepsilon (t-\tau)} E \right]_i d\tau \\ &= \frac{\delta}{\omega_o^4} \left(-A_\varepsilon^{-1} E + A_\varepsilon^{-1} e^{\omega_o A_\varepsilon t} E \right)_i \\ &\leq \frac{\delta}{\omega_o^4} \left\{ \left| (A_\varepsilon^{-1} E)_i \right| + \left| (A_\varepsilon^{-1} e^{\omega_o A_\varepsilon t} E)_i \right| \right\} \end{aligned} \quad (30)$$

As

$$A_\varepsilon^{-1} = \begin{bmatrix} 0 & 0 & 0 & -1 \\ 1 & 0 & 0 & -4 \\ 0 & 1 & 0 & -6 \\ 0 & 0 & 1 & -4 \end{bmatrix},$$

then

$$\left| \left[A_\varepsilon^{-1} E \right]_{i=1,2,3,4} \right| = \left| \begin{bmatrix} -1 \\ -4 \\ -6 \\ -4 \end{bmatrix} \right|_{i=1,2,3,4} \quad (31)$$

Since when $t > T_1$, $\left| \left[e^{\omega_o A_\varepsilon t} \right]_{ij} \right| \leq \frac{1}{\omega_o^4}$.

Let

$$A_\varepsilon^{-1} = \begin{bmatrix} b_{11} & b_{12} & b_{13} & b_{14} \\ b_{21} & b_{22} & b_{23} & b_{24} \\ b_{31} & b_{32} & b_{33} & b_{34} \\ b_{41} & b_{42} & b_{43} & b_{44} \end{bmatrix}, \quad \left| e^{\omega_o A_\varepsilon t} E \right| = \begin{bmatrix} a_{14} \\ a_{24} \\ a_{34} \\ a_{44} \end{bmatrix}$$

then

$$\begin{aligned} & \left| \left(A_\varepsilon^{-1} e^{\omega_o A_\varepsilon t} E \right)_{i=1,2,3,4} \right| \\ &= |b_{i1}a_{14} + b_{i2}a_{24} + b_{i3}a_{34} + b_{i4}a_{44}|_{i=1,2,3,4} \\ &\leq \frac{1}{\omega_o^4} (|b_{i1}| + |b_{i2}| + |b_{i3}| + |b_{i4}|) \\ &= \frac{7}{\omega_o^4} \end{aligned} \quad (32)$$

According to Eq. (31) and Eq. (32), the following equation can be obtained

$$\begin{aligned} |p(t)|_{i=1,2,3,4} &\leq \frac{\delta}{\omega_o^4} \left\{ \left| (A_\varepsilon^{-1} E)_i \right| + \left| (A_\varepsilon^{-1} e^{\omega_o A_\varepsilon t} E)_i \right| \right\} \\ &\leq \frac{\delta}{\omega_o^4} \left(6 + \frac{7}{\omega_o^4} \right) = \frac{6\delta}{\omega_o^4} + \frac{7\delta}{\omega_o^8} \end{aligned} \quad (33)$$

According to Eq. (29) and Eq. (33), then the following equation can be obtained

$$\begin{aligned} \varepsilon(t)_i &= e^{\omega_o A_\varepsilon t} \varepsilon(0)_i + \int_0^t \frac{Eh}{\omega_o^3} e^{\omega_o A_\varepsilon (t-\tau)} d\tau \\ &\leq \left| \left[e^{\omega_o A_\varepsilon t} \varepsilon(0) \right]_i \right| + |p_i(t)| \\ &\leq \frac{\varepsilon_{sum}(0)}{\omega_o^4} + \frac{6\delta}{\omega_o^4} + \frac{7\delta}{\omega_o^8} \end{aligned} \quad (34)$$

Let $e_{sum}(0) = |\tilde{e}_1(0)| + |\tilde{e}_2(0)| + |\tilde{e}_3(0)|$, then

$$|\tilde{e}_i(t)| \leq \frac{e_{sum}(0)}{\omega_o^4} + \frac{6\delta}{\omega_o^4} + \frac{15\delta}{\omega_o^8} = \mu \quad (35)$$

Eq. (35) shows that the estimated state errors are bounded and error monotonically decreases as the observer bandwidth increases.

Let e as the position tracking error, then the state of errors can be expressed as

$$e = [e_1 e_2 e_3]^T = [v_1 - z_1 v_2 - z_2 v_3 - z_3]^T$$

According to the state error equation of position tracking can be obtained from Eqs. (13) and (14) as follows

$$\dot{e} = A_e e + A_{\tilde{e}} \tilde{e} + B v_4 \tag{36}$$

where

$$A_e = \begin{bmatrix} 0 & 1 & 0 \\ 0 & 0 & 1 \\ -k_1 & -k_2 & -k_3 \end{bmatrix}, A_{\tilde{e}} = \begin{bmatrix} 0 & 0 & 0 \\ 0 & 0 & 0 \\ -k_1 & -k_2 & -k_3 \end{bmatrix},$$

$$B = \begin{bmatrix} 0 \\ 0 \\ 1 \end{bmatrix}, \text{ and } \begin{bmatrix} k_1 \\ k_2 \\ k_3 \end{bmatrix} = \begin{bmatrix} \omega_c^3 \\ 3\omega_c^2 \\ 3\omega_c \end{bmatrix}$$

Solving Eq. (36), the solution of $e(t)$ can be expressed as follows

$$e(t) = e^{A_e t} e(0) + \int_0^t e^{A_e(t-\tau)} (A_{\tilde{e}} \tilde{e} + B r_4) d\tau$$

$$= e^{A_e t} e(0) + \int_0^t e^{A_e(t-\tau)} d\tau + \int_0^t e^{A_e(t-\tau)} B r_4 d\tau \tag{37}$$

As $A_{\tilde{e}} \tilde{e}|_{i=1,2} = [0 \ 0 \ 0]^T [\tilde{e}_1 \ \tilde{e}_2 \ \tilde{e}_3]^T = 0$ and

$$A_{\tilde{e}} \tilde{e}|_{i=3} = \begin{bmatrix} -k_1 & -k_2 & -k_3 \end{bmatrix} \begin{bmatrix} \tilde{e}_1 \\ \tilde{e}_2 \\ \tilde{e}_3 \end{bmatrix}^T$$

$$= -k_1 \tilde{e}_1 - k_2 \tilde{e}_2 - k_3 \tilde{e}_3$$

$$\leq k_1 |\tilde{e}_1| + k_2 |\tilde{e}_2| + k_3 |\tilde{e}_3|$$

$$\leq (k_1 + k_2 + k_3) \mu$$

$$= \delta \tag{38}$$

Let $\varphi(t) = \int_0^t e^{A_e(t-\tau)} A_{\tilde{e}} \tilde{e} d\tau$, $\psi = [0 \ 0 \ \delta]^T$, the following equation can be derived

$$\varphi_i(t) = \int_0^t e^{A_e(t-\tau)} A_{\tilde{e}} \tilde{e} d\tau \Big|_i$$

$$\leq \int_0^t e^{A_e(t-\tau)} \psi d\tau \Big|_i$$

$$\leq |(A_e^{-1} \psi)_i| + |(A_e^{-1} e^{A_e t} \psi)_i| \tag{39}$$

As

$$A_e^{-1} = \begin{bmatrix} -\frac{k_2}{k_1} & -\frac{k_3}{k_1} & -\frac{1}{k_1} \\ 1 & 0 & 0 \\ 0 & 1 & 0 \end{bmatrix},$$

then

$$|(A_e^{-1} \psi)_i| = \left| \begin{bmatrix} -\frac{\delta}{k_1} \\ 0 \\ 0 \end{bmatrix} \right|.$$

Then the following equation can be derived

$$|(A_e^{-1} \psi)_i| = \begin{cases} -\frac{\delta}{k_1} = -\frac{\delta}{\omega_c^4}, & i = 1 \\ 0, & i = 2, 3 \end{cases} \tag{40}$$

Since A_e is Hurwitz, there exists $T_2 > 0$ so that $|(e^{A_e t})_{ij}| \leq \frac{1}{\omega_c^4}$.

Let $e^{A_e t} = \begin{bmatrix} c_{11} & c_{12} & c_{13} \\ c_{21} & c_{22} & c_{23} \\ c_{31} & c_{32} & c_{33} \end{bmatrix}$ and $e_{sum}(0) = \sum_{i=1}^3 |e_i(0)|$, then the following equation can be derived

$$\left| [e^{A_e t} e(0)]_{i=1,2,3} \right| = |c_{i1} e_1(0) + c_{i2} e_2(0) + c_{i3} e_3(0)|_i$$

$$\leq \frac{e_{sum}(0)}{\omega_c^4} \tag{41}$$

Let $T_3 = \max \{T_1 \ T_2\}$, then we can get the following equation:

$$|A_e^{-1} e^{A_e t} \psi| = \left| \begin{bmatrix} -\frac{3}{\omega_c} c_{13} - \frac{3}{\omega_c^2} c_{23} - \frac{1}{\omega_c^3} c_{33} \\ c_{13} \\ c_{23} \end{bmatrix} \right| \delta$$

$$\leq \begin{cases} \frac{3\omega_c^2 + 3\omega_c + 1}{\omega_c^7} \delta \Big|_{i=1} \\ \frac{\delta}{\omega_c^4} \Big|_{i=2,3} \end{cases} \tag{42}$$

For all $t \geq T_3$, substituting equations (40) and (42) into (39) yields

$$|\varphi_{i=1,2,3}(t)| \leq |(A_e^{-1} \psi)_i| + |(A_e^{-1} e^{A_e t} \psi)_i|$$

$$\leq \begin{cases} -\frac{\delta}{\omega_c^4} + \frac{3\omega_c^2 + 3\omega_c + 1}{\omega_c^7} \delta, & i = 1 \\ \frac{\delta}{\omega_c^4}, & i = 2, 3 \end{cases} \tag{43}$$

Assuming that $r_4 \leq \alpha$, then

$$|E r_4|_i = \begin{cases} 0, & i = 1, 2 \\ r_4 < \alpha, & i = 3 \end{cases} \tag{44}$$

Then the following equation can be obtained:

$$\int_0^t (e^{A_e(t-\tau)} E r_4) d\tau \leq \int_0^t (e^{A_e(t-\tau)} E \alpha) d\tau$$

$$= -A_e^{-1} e^{A_e(t-\tau)} E \alpha \Big|_0^t$$

$$= A_e^{-1} e^{A_e t} E \alpha - A_e^{-1} E \alpha \tag{45}$$

Since

$$|A_e^{-1} E \alpha|_i = \begin{cases} -\frac{\alpha}{k_1} = -\frac{\alpha}{\omega_c^3} & i=1 \\ 0, & i = 2, 3 \end{cases} \tag{46}$$

$$|A_e^{-1} e^{A_e t} E|_i \leq \begin{cases} \frac{3\omega_c^2 + 3\omega_c + 1}{\omega_c^7} \alpha, & i = 1 \\ \frac{\alpha}{\omega_c^4}, & i = 2, 3 \end{cases} \tag{47}$$

Then

$$\left| \left(\int_0^t e^{A_e(t-\tau)} E r_4 d\tau \right)_i \right| \leq \begin{cases} \frac{3\omega_c^2 + 3\omega_c + 1}{\omega_c^7} \alpha - \frac{\alpha}{\omega_c^3}, & i = 1 \\ \frac{\alpha}{\omega_c^4}, & i = 2, 3 \end{cases} \tag{48}$$

According Eqs. (43),(45)and (48), we can get the following equation

$$\begin{aligned}
 e(t) &= e^{A_e t} e(0) + \int_0^t e^{A_e(t-\tau)} A_{\tilde{e}} \tilde{e} d\tau + \int_0^t e^{A_e(t-\tau)} E r_4 d\tau \\
 &\leq \begin{cases} \frac{e_{sum}(0)}{\omega_c^4} - \frac{\delta + \alpha}{\omega_c^4} + \frac{3\omega_c^2 + 3\omega_c + 1}{\omega_c^7} (\delta + \alpha), & i = 1 \\ \frac{e_{sum}(0)}{\omega_c^4} + \frac{\delta + \alpha}{\omega_c^4}, & i = 2, 3 \end{cases}
 \end{aligned} \quad (49)$$

From the above analysis, the error is bounded and monotonically decreases as ω_c increases. Pressure controller stability proof is similar and is omitted here.

Statements and Declarations

No conflict of interest exists in the submission of this manuscript, and this manuscript is approved by all authors for publication

REFERENCES

- [1] D. Padovani, M. Rundo, and G. Altare, "The working hydraulics of valve-controlled mobile machines: Classification and review," *J. Dyn. Syst., Meas., Control*, vol. 142, no. 7, Jul. 2020, Art. no. 070801, doi: 10.1115/1.4046334.
- [2] K. Suzumori and A. A. Faudzi, "Trends in hydraulic actuators and components in legged and tough robots: A review," *Adv. Robot.*, vol. 32, no. 9, pp. 458–476, May 2018, doi: 10.1080/01691864.2018.1455606.
- [3] T. C. Do, T. D. Dang, T. Q. Dinh, and K. K. Ahn, "Developments in energy regeneration technologies for hydraulic excavators: A review," *Renew. Sustain. Energy Rev.*, vol. 145, Jul. 2021, Art. no. 111076, doi: 10.1016/j.rser.2021.111076.
- [4] K. Abuowda, I. Okhotnikov, S. Noroozi, P. Godfrey, and M. Dupac, "A review of electrohydraulic independent metering technology," *ISA Trans.*, vol. 98, pp. 364–381, Mar. 2020, doi: 10.1016/j.isatra.2019.08.057.
- [5] T. H. Nguyen, T. C. Do, and K. K. Ahn, "Research on a new independent metering system for boom excavator," in *Proc. 24th Int. Conf. Mechatronics Technol. (ICMT)*, Singapore, Dec. 2021, pp. 1–5, doi: 10.1109/ICMT53429.2021.9687258.
- [6] G. Chen, J. Wang, S. Wang, J. Zhao, and W. Shen, "Energy saving control in separate meter in and separate meter out control system," *Control Eng. Pract.*, vol. 72, pp. 138–150, Mar. 2018, doi: 10.1016/j.conengprac.2017.09.001.
- [7] J. Koivumaki, W. H. Zhu, and J. Mattila, "Energy-efficient and high-precision control of hydraulic robots," *Control Eng. Pract.*, vol. 85, pp. 176–193, Apr. 2019, doi: 10.1016/j.conengprac.2018.12.013.
- [8] C. Li, L. Lyu, B. Helian, Z. Chen, and B. Yao, "Precision motion control of an independent metering hydraulic system with nonlinear flow modeling and compensation," *IEEE Trans. Ind. Electron.*, vol. 69, no. 7, pp. 7088–7098, Jul. 2022, doi: 10.1109/TIE.2021.3102434.
- [9] W. Liu, Y. Li, and D. Li, "A coordinated control law for inlet/outlet independent regulation of electro-hydraulic speed control system under sustained negative load," *Proc. Inst. Mech. Eng., C, J. Mech. Eng. Sci.*, vol. 234, no. 9, pp. 1689–1705, May 2020, doi: 10.1177/0954406219899691.
- [10] Z. Liu, B. Jin, J. Dong, S. Zhai, and X. Tang, "Design and control of a hydraulic hexapod robot with a two-stage supply pressure hydraulic system," *Machines*, vol. 10, no. 5, p. 305, 2022.
- [11] Q. Liu, H. Du, Z. Cai, K. Guo, and J. Fang, "Application research of electro-hydraulic servo steering system based on independent metering system," *Proc. Inst. Mech. Eng., D, J. Automobile Eng.*, Nov. 2022, Art. no. 095440702211395, doi: 10.1177/09544070221139553.
- [12] J. Yao, "Model-based nonlinear control of hydraulic servo systems: Challenges, developments and perspectives," *Frontiers Mech. Eng.*, vol. 13, no. 2, pp. 179–210, Jun. 2018.
- [13] J. Han, "From PID to active disturbance rejection control," *IEEE Trans. Ind. Electron.*, vol. 56, no. 3, pp. 900–906, Mar. 2009.
- [14] A. J. Humaidi and H. M. Badr, "Linear and nonlinear active disturbance rejection controllers for single-link flexible joint robot manipulator based on PSO tuner," *J. Eng. Sci. Technol. Rev.*, vol. 11, no. 3, pp. 133–138, Apr. 2018, doi: 10.25103/jestr.113.18.
- [15] W. Lu, Q. Li, K. Lu, Y. Lu, L. Guo, W. Yan, and F. Xu, "Load adaptive PMSM drive system based on an improved ADRRC for manipulator joint," *IEEE Access*, vol. 9, pp. 33369–33384, 2021, doi: 10.1109/ACCESS.2021.3060925.
- [16] Z. Xu and C. Gerada, "Enhanced estimation of clamping-force for automotive EMB actuators using a switching extended state observer," *IEEE Trans. Ind. Electron.*, vol. 71, no. 3, pp. 2220–2230, Mar. 2024, doi: 10.1109/TIE.2023.3265060.
- [17] Z. Pan, X. Wang, Z. Zheng, and L. Tian, "Fractional-order linear active disturbance rejection control strategy for grid-side current of PWM rectifiers," *IEEE J. Emerg. Sel. Topics Power Electron.*, vol. 11, no. 4, pp. 3827–3838, Aug. 2023, doi: 10.1109/JESTPE.2023.3264481.
- [18] S. Li, J. Yang, W.-H. Chen, and X. Chen, "Generalized extended state observer based control for systems with mismatched uncertainties," *IEEE Trans. Ind. Electron.*, vol. 59, no. 12, pp. 4792–4802, Dec. 2012, doi: 10.1109/TIE.2011.2182011.
- [19] C. Wang, L. Quan, S. Zhang, H. Meng, and Y. Lan, "Reduced-order model based active disturbance rejection control of hydraulic servo system with singular value perturbation theory," *ISA Trans.*, vol. 67, pp. 455–465, Mar. 2017.
- [20] H. Jingqing, *Active Disturbance Rejection Control Technique—The Technique for Estimating and Compensating the Uncertainties*. Beijing, China: National Defense Industry Press, Sep. 2008.
- [21] X. Wang, Z. Chen, and Z. Yuan, "Design and analysis for new discrete tracking-differentiators," *Appl. Math. A J. Chin. Universities*, vol. 18, no. 2, pp. 214–222, Jun. 2003, doi: 10.1007/s11766-003-0027-0.
- [22] Z. Gao, "Scaling and bandwidth-parameterization based controller tuning," in *Proc. Amer. Control Conf.*, Jun. 2003, pp. 4989–4996.
- [23] H. Zhang, S. Zhao, and Z. Gao, "An active disturbance rejection control solution for the two-mass-spring benchmark problem," in *Proc. Amer. Control Conf. (ACC)*, Jul. 2016, pp. 1566–1571.
- [24] D. Yoo, S. S.-T. Yau, and Z. Gao, "On convergence of the linear extended state observer," in *Proc. IEEE IEEE Conf. Comput. Aided Control Syst. Design Int. Conf. Control Appl. Int. Symp. Intell. Control, Oct. 2006*, pp. 1645–1650, doi: 10.1109/CACSD-CCA-ISIC.2006.4776888.



WANG MENG received the B.S. degree from the Taiyuan Institute of Technology, in 2013, and the M.S. degree from the Taiyuan University of Science and Technology, in 2016, where he is currently pursuing the Ph.D. degree. His research interests include electro-hydraulic servo control and energy recovery.

LI HUSHAN, biography not available at the time of publication.



GAO YOUSHAN received the Ph.D. degree from Beihang University, in 2009. He is currently a Professor with the School of Mechanical Engineering, Taiyuan University of Science and Technology. His research interests include electro-hydraulic servo control and energy recovery.

XI HAO, biography not available at the time of publication.